2007-03

Automating the shadow method for aerosol optical depth retrieval

Dombrock, Ryan M.

Monterey, California. Naval Postgraduate School

NAVAL POSTGRADUATE SCHOOL

MONTEREY, CALIFORNIA

THESIS

AUTOMATING THE SHADOW METHOD FOR AEROSOL OPTICAL DEPTH RETRIEVAL

by

Ryan M. Dombrock

March 2007

Thesis Advisor:	P. A. Durkee
Second Reader:	K. E. Nielsen

THIS PAGE INTENTIONALLY LEFT BLANK

REPORT DOCUMENTATION PAGE		Form Approved OMB No. 0704-0188

1. AGENCY USE ONLY *(Leave blank)*	2. REPORT DATE	3. REPORT TYPE AND DATES COVERED
	March 2007	Master's Thesis

4. TITLE AND SUBTITLE Automating the Shadow Method for Aerosol Optical Depth Retrieval	5. FUNDING NUMBERS
6. AUTHOR(S) Ryan M. Dombrock	
7. PERFORMING ORGANIZATION NAME(S) AND ADDRESS(ES) Naval Postgraduate School Monterey, CA 93943-5000	8. PERFORMING ORGANIZATION REPORT NUMBER
9. SPONSORING /MONITORING AGENCY NAME(S) AND ADDRESS(ES) N/A	10. SPONSORING/MONITORING AGENCY REPORT NUMBER

11. SUPPLEMENTARY NOTES The views expressed in this thesis are those of the author and do not reflect the official policy or position of the Department of Defense or the U.S. Government.

12a. DISTRIBUTION / AVAILABILITY STATEMENT	12b. DISTRIBUTION CODE
Approved for public release; distribution is unlimited	

13. ABSTRACT (maximum 200 words)

A new method for remote sensing retrieval of Aerosol Optical Depth was proposed and investigated by Vincent (2006). This shadow-based method uses the radiance difference between shadow and non-shadow regions in QuickBird high resolution commercial satellite imagery to estimate Aerosol Optical Depth. Though the process is initially time-consuming, requiring a high level of user knowledge to accomplish the procedure, great potential exists for further development into a stand-alone operational method for overland retrievals at any location and time. It is the automation of this process in order to make it more operational in nature that is the purpose of this investigation. Knowledge is gained in the realm of predicting shadow location for future times. Specific process automation is applied through computer programming to decrease the computational complexity of the method. Also the physical variations of shadow regions are investigated in terms of their brightness change across various spatial profiles. This study of shadow region variation is termed shadow morphology and seeks to provide a user with optimum radiance sampling regions within an observed shadow region. Through the integration of these automation techniques, a more unified and operationally focused iteration of the shadow method is derived.

14. SUBJECT TERMS	15. NUMBER OF PAGES
Aerosol, Aerosol Optical Depth Retrieval, Shadow Morphology, Automation, Over Land, Shadow, High-Resolution Commercial Satellite Imagery, QuickBird	59
	16. PRICE CODE

17. SECURITY CLASSIFICATION OF REPORT	18. SECURITY CLASSIFICATION OF THIS PAGE	19. SECURITY CLASSIFICATION OF ABSTRACT	20. LIMITATION OF ABSTRACT
Unclassified	Unclassified	Unclassified	UL

NSN 7540-01-280-5500 Standard Form 298 (Rev. 2-89)
Prescribed by ANSI Std. 239-18

THIS PAGE INTENTIONALLY LEFT BLANK

Approved for public release; distribution is unlimited

AUTOMATING THE SHADOW METHOD FOR AEROSOL OPTICAL DEPTH RETRIEVAL

Ryan M. Dombrock
Second Lieutenant, United States Air Force
B.S., United States Air Force Academy, 2005
B.S., Naval Postgraduate School, 2006

Submitted in partial fulfillment of the
requirements for the degree of

MASTER OF SCIENCE IN METEOROLOGY

from the

NAVAL POSTGRADUATE SCHOOL
March 2007

Author: Ryan M. Dombrock

Approved by: Philip A. Durkee
Thesis Advisor

Kurt E. Nielson
Second Reader

Philip A Durkee
Chairman, Department of Meteorology

THIS PAGE INTENTIONALLY LEFT BLANK

ABSTRACT

A new method for remote sensing retrieval of Aerosol Optical Depth was proposed and investigated by Vincent (2006). This shadow-based method uses the radiance difference between shadow and non-shadow regions in QuickBird high resolution commercial satellite imagery to estimate Aerosol Optical Depth. Though the process is initially time-consuming, requiring a high level of user knowledge to accomplish the procedure, great potential exists for further development into a stand-alone operational method for overland retrievals at any location and time. It is the automation of this process in order to make it more operational in nature that is the purpose of this investigation. Knowledge is gained in the realm of predicting shadow location for future times. Specific process automation is applied through computer programming to decrease the computational complexity of the method. Also the physical variations of shadow regions are investigated in terms of their brightness change across various spatial profiles. This study of shadow region variation is termed shadow morphology and seeks to provide a user with optimum radiance sampling regions within an observed shadow region. Through the integration of these automation techniques, a more unified and operationally focused iteration of the shadow method is derived.

THIS PAGE INTENTIONALLY LEFT BLANK

TABLE OF CONTENTS

THIS PAGE INTENTIONALLY LEFT BLANK

LIST OF FIGURES

LIST OF TABLES

THIS PAGE INTENTIONALLY LEFT BLANK

ACKNOWLEDGMENTS

The completion of this thesis would have been altogether impossible without the assistance, contributions, and support of various individuals. I would like to thank my advisor, Prof. Philip A. Durkee, for providing the inspiration for this work as well as immeasurable guidance throughout the thesis process. Kurt Nielsen's input to my general understanding of the shadow-method and its process helped me get off the ground, and his advice, hard work, friendship, and drama suppression carried me through to the end. Capt. Jack Evans was a valuable asset providing operational testing of my automation work in his own thesis work. He also served as a very effective sounding board and sanity check as we strove towards the same ultimate goal for the shadow method. Prof. Durkee, Kurt, and Capt. Evans also generously sacrificed of their own time and equipment in order to accomplish the field study for shadow morphology and I could not have accomplished the analysis without them.

Though the single Lt. lacks the typical military family to thank, this lucky one did have his own very effective support structure and a loving mix of family and friends were invaluable to my success and survival. My parents, Arlen and Patricia Dombrock, took an active roll in listening to all the thesis ideas, problems, confusions, and apprehensions I had. More importantly though I could not have reached where I am today without them and any success I have had in life has been a direct result of the amazing foundation, support, and encouragement they have provided me with. I thank my brother, Kevin, who as a student himself understood and related to my occasional academic frustrations. He is also a great source of inspiration as I am constantly trying to live up to the high esteem he holds for me. To Melissa, who blazed the thesis path before me and always believes in me when my own faith wavers, I am incredibly grateful for your continued love and support. I would like to thank my roommate, Eric Cercone, who saved me from homelessness, became a friend, and provided many rides to school. I am also thankful to all my NPS classmates and faculty who helped pull this weather "newbie" through the BMP program and supported my extension into the Master's program.

THIS PAGE INTENTIONALLY LEFT BLANK

I. INTRODUCTION

A. MOTIVATION

Characterization of atmospheric aerosols has proven a difficult task due to the highly varied nature of their spatial and temporal distributions throughout the atmosphere. These aerosols have the potential to influence military operations at many levels, and of particular concern is the measurement of aerosol optical depth within theaters of operation. Atmospheric aerosols scatter energy at both visible and near-infrared wavelengths and thus have a diverse range of effects (Martin 2004). Aerosol optical depth can be directly correlated to visibility and provide insight into the feasibility of many mission types ranging from aircraft flight to troop movement. Indirectly, aerosol optical depth is an important factor in the functionality of many types of electro-optical systems which encompass systems such as communications and targeting platforms. The physical deterioration of electro-optical signals by scattering aerosols in the atmosphere is of concern to the operators of such systems in the form of transmittance calculations (AFRL 2004, Higgins *et al.* 1989). Due to the fact that in situ measurement of aerosol optical depth requires expensive equipment that would not be highly transportable to a given area of operations or areas with restricted access, the creation of a highly automated method of sensing aerosol optical depth from existing remote sensing platforms is desirable and necessary for timely detection of such an important parameter at any global location. The development of this remote sensing method can provide direct benefit to the war fighter in his area of operations and contribute to higher mission success rates.

B. OBJECTIVES

The primary objective of this study is to facilitate research by automating an existing remote sensing method for measuring aerosol optical depth using high resolution commercial satellite imagery. The shadow-based method for remote sensing of aerosol optical depth outlined by Vincent (2006) will provide the groundwork for this study with

the goal of making this method more functional in an operational environment. Many areas of automation and research into various aspects of the technique are required to make this method feasible for operational use by the war fighter.

Automation techniques will be applied to the specific method of calculating optical depth from satellite imagery, and an analysis of shadow-generators, geometry, and shadow regions will be provided. Specific attention will be paid to the way in which both solar and satellite geometries interact to produce shadow regions from interaction with shadow-generators, with particular attention paid to how these shadow regions can then be predicted in time, location, and spatial dimensions. Furthermore, a greater understanding of the shadow regions themselves is necessary to facilitate accurate and more efficient sampling of shadow regions from satellite imagery. The spatial variation of radiance within the shadow region across its dimensions, termed shadow morphology, and the various factors affecting these variations will be the primary area of investigation into the shadow region analysis.

With a more comprehensive understanding of the shadow region spatial variations, aerosol optical depth calculation using shadow and non-shadow radiance differencing can be enhanced in both consistency and accuracy. Reduction in the physical time of analysis for a user to perform an aerosol optical depth calculation from satellite imagery using the shadow method will enhance further research into the method and its validity. Better understanding of shadow production through geometric interactions will allow for easier shadow location and dimensional prediction, and knowledge of shadow morphology will provide guidance on the sampling of shadow regions. Though several distinctly different areas will be investigated, the overall combined effect of the following analysis works to further the operational functionality of the shadow-based aerosol optical depth retrieval method using high resolution commercial satellite imagery.

II. BACKGROUND

A. RELATED RESEARCH

Creation of comprehensive AOD retrievals applicable to all situations over land areas have proven difficult. The variations inherent in land surface backgrounds produce the difficulties behind retrieval shortfalls such as channel saturation and surface complexity. A summary of three areas of research into AOD characterization over land is provided below, outlining the most accepted methods for retrieval.

1. Contrast Reduction Methods

The adding method for radiative transfer was applied to radiance differences between objects of different albedo by Odell and Weinman (1975) to create a relationship to AOD. A computationally expensive method for complex aerosol regimes, the method was deeply rooted in a contrast transmission function based on AOD, surface reflectance, and solar and sensor geometry. Target pixels and background pixel signals were partitioned by Tanre *et al.* (1981) to create a space-based ground reflectance correction algorithm and to characterize background influence. An automated procedure produced by Kaufman and Joseph (1982) was able to separate visible satellite imagery into fields of different albedos using a step discontinuity for surface albedo to derive atmospheric extinction and was successful for imagery with high-spatial resolution. The procedure was highly influenced by AOD and single scatter albedo, however, it was insensitive to radiance measurement errors. The brightening influence of highly reflective pixels on nearby dark pixels, or "adjacency effect", was described by Kaufman and Fraser (1984) in terms of its proportionality to aerosol scale height. Successful application of contrast reduction using histogram variance of surface reflectance over an assumed constant ground reflectance to Saharan dust cases was obtained by Tanre *et al.* (1988), however, assumptions about aerosol characterization were still needed for use in transmission functions.

2. Dark Object Method

The dark object method contends that surface reflectance can be neglected over a sufficiently dark surface object leaving the remaining measured radiance due to aerosol scattering path radiance. This technique is applied to dense vegetation (Kaufman and Sendra 1988) and inland bodies of water (Kidder and Vonder Haar 1999). Success is possible with this method over certain regions containing the proper surface characteristics. However, desert and urban regions often exhibit consistent high surface reflectances and lack large deep water features. A "Deep Blue" method used by Hsu *et al.* (2004) took advantage of multiple blue bands in SeaWiFS and MODIS imagery to take advantage of lower surface reflectance for these wavelengths over areas with bright surfaces in other bands. The high sensitivity of the blue bands to dust property variations coupled with the use of a coarse grid database of surface reflectance lead to uncertainties for this retrieval. Also, higher resolution satellites typically lack multiple bands in blue wavelengths rendering this approach unfeasible.

3. Multi-Angle Method

Satellites with multi-view capabilities can be used to characterize surface reflectance from multiple measurements of radiance of the same surface. A variety of aerosol properties are modeled to create values for the atmospheric contribution. A complementary combination of modeled atmospheric and measured surface reflectances is then derived to match top of the atmosphere reflectance. The Along Track Scanning Radiometer 2 (ATSR-2) and Multi-angle Imaging SpectroRadiometer (MISR) are two sensors reported to have success with this method by Veefkind *et al.* (1998) and Martonchik *et al.* (2004) respectively. Timely operational AOD retrievals would prove difficult using this method, however, due to difficulty in aerosol modeling and the lack of high-resolution satellites with multi-view capabilities (Vincent 2006).

B. SHADOW METHOD

A new method for remote sensing of aerosol optical depth (AOD) retrieval is proposed and studied by Vincent (2006) to overcome shortfalls in other overland

methods. The shadow-based method uses radiance differences between shadow and non-shadow areas in QuickBird commercial, high-resolution satellite imagery to calculate optical depth. Surface reflectance values of at least 0.15 over a uniform surface were necessary for valid results. External data sets, such as surface reflectance databases and complex aerosol model tables, were not required for this method making it a single stand-alone procedure. From a collection of multiple AOD retrievals across a single satellite image, an average AOD was calculated and then compared with nearby AERONET AOD measurements for the time nearest to the imaging time. Desert, urban, and grass backgrounds were investigated.

In the desert background investigation by Vincent (2006), the panchromatic channel exhibited a consistent low bias. The multi-spectral results matched well with AERONET AOD data. For urban cases, large low bias in the retrieved AOD was present and was enhanced by the blocking of sky irradiance by multiple adjacent structures. Over grass backgrounds, blue and near-infrared channels provided good results while other channels showed low bias. Surface reflectance values over grass backgrounds were too low in the blue, red and green channels for good results to be obtained, however, in the blue channel higher levels of solar irradiance compensated for low reflectance to provide realistic retrievals. For all retrieval categories a correction of the final AOD to account for gaseous absorption improved AOD results.

The theoretical development of the shadow-based method followed Liou's (2002) principles-of-invariance method of radiative transfer. An irradiance balance is created with upward irradiance equaling surface reflectance multiplied by downward irradiance.

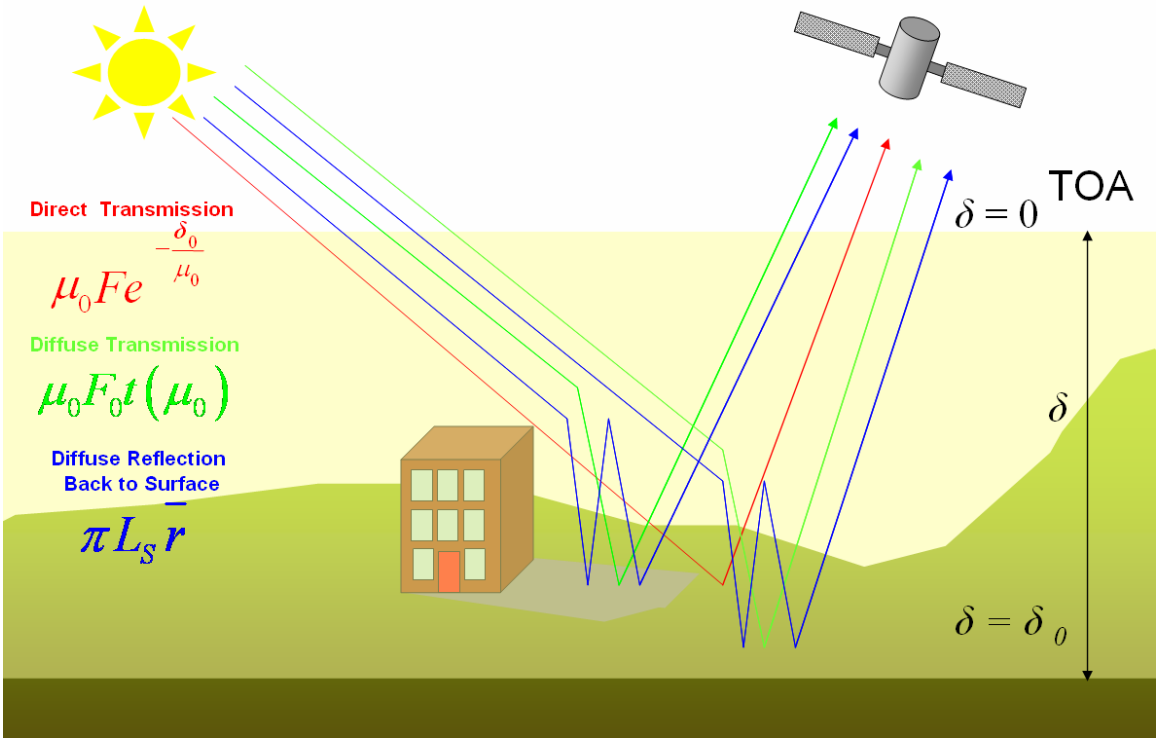

Figure 1. Direct transmission and total optical depth is quantified by the shadow method using the radiances differences between shadow and non-shadow regions. (from Vincent 2006)

The key quantities of downward irradiance are displayed in Fig. 1 noting the important difference that for shadow regions the direct transmission term, present for non-shadow regions, is eliminated. The equation can then be solved for surface radiance once the parameters responsible the terms of the irradiance balance relationship are specified. Adding an additional extinction term to account for the path loss by optical depth between the surface and the satellite sensor, the equation then accounts for satellite-measured surface radiance. When measuring shadow areas in an image the direct transmission term is removed and only radiance from diffuse transmission and atmosphere reflected surface radiance remain. Due to this relationship, the difference between physically measured radiance between a non-shadow and shadow region over a uniform surface can then be set equal to only the direct transmission term. Knowing the

direct transmission value from the radiance difference, the equation can then be solved for total optical depth as shown in final form in Eq. (1).

$$\delta_0 = \left(\frac{\mu_0 \mu}{\mu + \mu_0} \right) \ln \left[\left(\frac{r_s}{1 - r_s \bar{r}} \right) \left(\frac{\mu_0 F_0}{\pi L_d} \right) \right] \tag{1}$$

To retrieve an aerosol optical depth from the satellite imagery, top of the atmosphere reflectance is at first assumed to represent surface reflectance. From a first iteration, the total optical depth calculation based on the non-shadow and shadow radiance difference in the imagery, a mean aerosol reflectance is calculated. This mean aerosol reflectance value is then subtracted from the initial assumed surface reflectance to divide the top of the atmosphere reflectance into surface and mean aerosol reflectance components. Eq. (1) is then used to retrieve the second iteration of total optical depth using the new surface reflectance value. Finally, a band-specific correction to account for optical depth due to molecular Rayleigh scattering is calculated and subtracted from the total optical depth to determine aerosol optical depth.

THIS PAGE INTENTIONALLY LEFT BLANK

III. DATA AND METHODOLOGY

A. SHADOW PREDICTION

The ability to predict the location of shadows is required in order to pursue a fixed targeting strategy for automating the shadow method for AOD retrieval. In the fixed targeting strategy, certain shadow producers would be identified for a given location and information about their dimensions would be used to automatically identify their shadow regions for any given time. The first area of investigation involved using orbital prediction software to predict coverage times, solar angles, and satellite viewing angles. Secondly, shadow-containing imagery was analyzed to investigate the physical prediction of shadow length and location.

1. Data

The data used for the building height and shadow prediction area of this study included Quickbird (QB) commercial satellite imagery data and two-line element (TLE) data retrieved from the Satellite Tool Kit Software (STK) (Analytical Graphics, Inc. 2007). The STK software contains QB orbital specifications within its database and can automatically update TLE data for increased accuracy of orbital data. With this feature, the location and geometry of QB can be calculated for a given time in its orbital history or for a future time period. Vector calculation tools within the software provide angular data between both the satellite and the sun in relation to a user defined ground target. QB orbits the Earth in a 98 degree sun-synchronous orbit at an altitude of 450 kilometers with a revisit time of 1 to 3.5 days depending on the latitude of interest (DigitalGlobe 2006). A sun-synchronous orbit provides satellite passes at the same local solar time for a given point. The benefit of the sun-synchronous orbit is to maintain nearly constant solar geometry and lighting characteristics over a variety of passes. QB provides the platform for the very high resolution satellite imagery, however, more specifically it is the Ball Global Imaging System 2000, or BGIS 2000, instrument that physically creates the imagery. Two sub-systems comprise BGIS 2000 - the Ball High Resolution Camera 60

and a spacecraft bus called the Ball Commercial Platform 2000. The pushbroom camera provides for flexibility in imaging with retargeting capability and multiple image types including square images, elongated strip images, mosaic patterns, and stereo pairs within a single pass (Ball Aerospace 2006). As applied to the QB platform, the sensor provides 0.6 meter panchromatic and 2.44 meter multispectral resolution at nadir - the highest resolution commercially available (Digital Globe 2006). The multispectral bands include blue, green, red, and near infrared wavelengths with the panchromatic band spanning the multispectral bands from 445 to 900 nanometers. The sensor has nominal swath width of 16.5 kilometers at nadir with an accessible ground swath of 544 kilometers. Single area images are produced in 16.5 kilometer squares, or strip imaging can produce 16.5 kilometer by 165 kilometer images (DigitalGlobe 2006). The features provided by the Ball High Resolution Camera 60 create extremely accurate imaging over a relatively broad footprint, provide flexibility for tailored collections, and allow for a variety of analysis techniques using its five multi-spectral bands. For the shadow area investigation, two standard 16.5 by 16.5 kilometer QB images were used, and the analysis was accomplished using Research Systems Inc's Environment for Visualizing Images Software (ENVI). ENVI provides a platform for orthorectification of the imagery and calibration of the spectral bands, which allows for accurate spatial and spectral analysis.

2. Orbital Prediction

Orbital prediction is an important component of automating AOD retrieval by the shadow-based method. In order to correctly predict the spatial and temporal locations of shadows for automatic computation, it is necessary to first predict satellite coverage and the geometric relationships inherent to the coverage. Using STK software data, the solar and sensor geometries were calculated for times corresponding to QB imaging and then compared to the actual angular data from the QB collection.

3. Scene Comparison

A remote calculation of shadow-producers is a necessary first step in order to predict shadow locations for given scenes, The interaction of solar and sensor geometry can be used to predict the size and shape of the shadows produced by a structure for future times once building height is determined. To investigate this relationship, two separate QB images for the same location in Beijing, China were compared for building height prediction and shadow location prediction testing. Either the building height can be predicted from a measured shadow length or the shadow length can be predicted from a known building height using the angular relationships shown in Fig. 2.

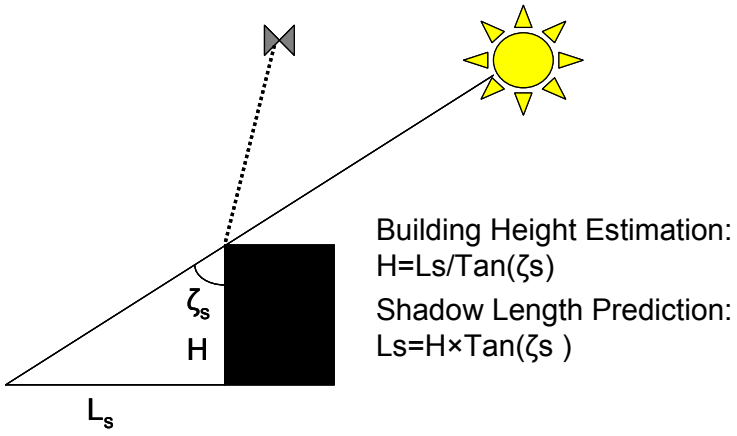

Figure 2. Building height and shadow length can be related with solar zenith angle.

The images chosen were from 13 September 2003 and 27 October 2003, and two distinct buildings were chosen as the targets for the analysis. With the different geometries present for these two scenes, a comparison of the building height estimation using the same buildings was possible as well as a test of the shadow prediction method.

B. AUTOMATING PROCESS

The automation of the physical process for performing the shadow-based AOD retrieval using QB satellite imagery required computer programming to unite the process in one streamlined step within the imagery analysis software. For a fully automated method to be implemented operationally, it is imperative to decrease both total

calculation time and required user input. These improvements are also highly beneficial to the future research into the process as speed and ease of analysis leads to an increase in the number of cases that can be analyzed in a variety of research capacities. At this time, it is beyond the scope of knowledge and software capabilities to automatically define shadow and non-shadow regions for an image. Thus the end-state for this research will be to provide a program which will take user-defined shadow and non-shadow regions, and automatically provide the retrieved AOD in one manual step.

1. Data

The data required for the automation process was the orthorectified and calibrated QB imagery in all five bands. Data and calculations provided by Vincent (2006) from the development and testing of the shadow-based AOD method were necessary also for insight into the physical workings of the method. Statistics provided by the ENVI software provides the starting point for AOD retrieval by automatically calculating radiance values of shadow and non-shadow regions. With the union of this information and the knowledge contained in the ENVI Programmers Guide (1999), a singular calculation method is created.

2. Previous Process

To describe the development of the automated process, it is first necessary to understand the previous method of imagery analysis to retrieve AOD. The investigation and understanding of the original process allows for insight into the areas in which automation is required and possible. The first step for the retrieval of AOD using the shadow-based method was the visual inspection of an image for shadow region identification. Once usable shadows were identified, region of interest (ROI) pairs were hand-drawn within the ENVI software corresponding to shadow and non-shadow regions for a given shadow. The ENVI statistics program was then run to provide data from the ROIs such as the minimum, maximum, mean, and standard deviation of radiance values. For the panchromatic channel ENVI-created histograms were used to hand-select a mode value for the radiance of the shadow regions. These radiance values were then hand-

copied into a spreadsheet. Once all the data was compiled in the spreadsheet for a given scene, the data was then manually transferred into a user-defined array in an IDL computer program designed to then calculate AOD from the retrieved radiance values. Clearly this method requires a high amount of user input, and also physical modification of the AOD calculating program is necessary for each new scene.

3. Automated Process

The goal of the automated process is to decrease the user input, create a single reusable IDL program for all scenes, and decrease the overall processing time of the shadow-based AOD retrieval method. As the ENVI statistics program is already used for calculating radiance values and IDL is the parent language for the ENVI software, it is possible to create a single interface in ENVI for the entire retrieval method. Combining the ENVI statistics and IDL program with the AOD retrieval program created by Vincent (2006), using a fixed array for the calculation of AOD for one ROI at a time, and building program widgets to prompt for user inputs of solar and satellite zenith angles as well as ROI selection creates a single program for the entire AOD retrieval within ENVI. The user can now create ROIs for the shadow and non-shadow regions, run the program for those regions, and obtain AOD values in one step while still viewing the imagery. Data collection for multiple ROIs within a scene is as simple as copying the IDL AOD output into whatever database the user chooses. Calculations for the panchromatic channels, however, cannot use the user-selected mode values as before because they cannot be automatically calculated and properly selected by the software. Nonetheless, a platform now exists from which a user can select shadow and non-shadow regions from a QB image and retrieve AOD values in one step provided enough information is known about proper selection of these regions for accurate analysis. The goal of the following section is to provide further insight into the shadow morphology to allow for shadow-region selection that will provide more accurate AOD retrieval.

C. SHADOW MORPHOLOGY

To understand the true nature of the spatial variations in radiance values across a shadow region, a very high spatial resolution study was necessary on orders of magnitude higher than available from the satellite imagery. To accomplish this goal, two experiments were designed using digital cameras to image shadow regions over relatively uniform surfaces. The Marina, California, airport was the site for both experiments as it provided access to various surface types and hanger roof access for shadow imaging.

Quantifiable radiance values are not calculated from the digital photographs, though qualitative analysis of variations is possible across three bands provided by the digital cameras. The brightness counts for the red, green, and blue bands provided from the images are used to approximate radiance values for these wavelengths. Two different cameras were used for the studies, a Canon EOS 20D and a Nikon D200 set at 72 dpi and 300 dpi horizontal and vertical resolutions respectively. The digital imagery was saved in standard JPEG format and analyzed with the same ENVI software used for the aerosol optical depth calculations. In the ENVI program, the images are loaded and, using the arbitrary profile tool, shadow region profiles showing the spatial variation of the three bands are created.

The ENVI profile output is saved as ASCII files for each profile which can then be imported into Microsoft Excel and plotted in a variety of ways for qualitative comparison. Excel functions also allow for some quantitative comparisons between profiles. The flexibility of this profiling method allows for characterization of shadow regions in various ways. Profiling is accomplished in both the vertical and horizontal directions across the shadow region as well as profiling the same surface area at different times and while it is in and out of the shadow region. The two distinct experiments were designed to analyze different aspects of shadow morphology. The first was more concerned with shadow evolution, and the second with purely spatial variations under the influence of different conditions.

1. Fixed Building Experiment

The first experiment took place on 29 November 2006 and featured both the Canon EOS 20D and Nikon D200 cameras affixed on tripods to the Northeast corner of the Naval Postgraduate School's Center for Interdisciplinary Remotely-Piloted Aircraft Studies (CIRPAS) hangar at the Marina, CA airport.

Figure 3. The shadow view from CIRPAS hangar for the 29 November 2006 study shows the surface area over which the shadow progressed during the study.

Figure 3 shows an example image from the study. Images were taken from both cameras simultaneously every ten minutes from 1130 to 1550 local time to image the evolution of the shadow cast by the hangar throughout the afternoon. Handheld sunphotometer measurements were also collected to provide an in situ measurement of aerosol optical depth during the experiment. The Canon EOS 20D manually held constant f11 aperture and 1/100 second shutter speed settings throughout the experiment, so that subsequent images could be compared for analysis while the Nikon D200 varied its aperture to avoid image washout and allow coherent analysis of the shadow region profiles at a single given time. Two different surface types were available within the shadow region as the early shadow was over a primarily asphalt surface and as the day

progressed the shadow moved over a brighter concrete tarmac surface. A downfall of the first experiment was that due to camera angles and the large shadow cast by the hangar, imaging of the entire shadow region was impossible. Also, the extent of the shadow region nearest the building was not available in the imagery due to the camera angle. To remedy these issues and investigate other variables, the second experiment was needed.

2. Manufactured Shadow Studies

A portable shadow-generator was created in the form on a 4 by 12 foot sheet of plywood with the goal of imaging entire shadow regions and manipulating specific variables. The variables of interest included ground surface type within the shadow region, surface brightness of the shadow producer, and shadow producer orientation. One side of the plywood was painted black and the other white to alternatively simulate low and high reflective shadow-generating buildings. Figure 4 displays a typical image setup for this experiment with the board oriented horizontally over asphalt with the bright surface facing the shadow region.

Figure 4. The plywood shadow-generator used for the 6 December 2006 is shown in the horizontal orientation with its bright surface facing the shadow region. The alternate dark side was used and orientations were varied over three different surface types for analysis.

The plywood could be rotated in either a horizontal of vertical orientation to compare the affects of building aspect ratios to the influence it creates on shadow morphology. This manufactured shadow-generator was also highly portable and could be moved onto the various ground surface types available at the Marina airport. Three surface types were imaged on the experiment date of 6 December 2006: the concrete tarmac, newer more uniform asphalt, and older highly variable asphalt. The concrete tarmac provided a relatively uniform bright surface, the newer asphalt provided a relatively uniform dark surface, and the old asphalt represented a dark surface with variable bright components due to the highly reflective characteristics of some of its aggregate materials. The imager for this study was the Canon D200 using a manually fixed f8 aperture. Images were taken from 1430 to 1500 local time beginning with the new asphalt and ending with the old asphalt. For each surface type, the plywood shadow-generator was rotated from horizontal to vertical orientation with both the black and white sides imaged in each orientation. In each image the entire shadow region is available for analysis as well as the corresponding non-shadow areas adjacent to the shadow boundaries.

Again for analysis, the JPEG images were loaded into the ENVI software and six profiles created for each image. Three horizontal profiles across the shadow region near the shadow producer, in the center, and at the shadow extent were created. Also three vertical profiles were created from the base of the board outward in the center and at each horizontal edge. With the vertical orientation of the plywood at the end of the longer shadow, the camera produced lens flares biasing the results of these long profiles. However, the transition region near the base of the board is still valid for analysis.

THIS PAGE INTENTIONALLY LEFT BLANK

IV. RESULTS

A. SHADOW PREDICTION

Results from the comparison of identical targets within two separate QB scenes from Beijing on 13 September 2003 and 27 October 2003 show that the proposed geometric relations hold, provided the building edge is visible and the shadow region is not obscured by the building itself or adjacent structures. The heights of the two buildings were calculated for each scene using the STK predicted geometry from the respective date and time to judge the performance of this building height estimation method. Results are listed in Table 1 comparing the heights of each building calculated from the separate images. Despite different geometries and shadow lengths, the two scenes estimate building heights to within a half meter of each other using this method.

Table 1. Calculated height estimates are listed along with the measured shadow lengths and geometry used to calculate them from the QuickBird satellite imagery. The two target buildings in Beijing, China are identified as is the imagery collection date of either 13 September or 27 October 2003.

	13 Sep Building 1	27 Oct Building 1	13 Sep Building 2	27 Oct Building 2
Solar Z	40.3	55.7	40.3	55.7
Solar Az	148.0	156.4	148.0	156.4
Sat Z	14.7	33.1	14.7	33.1
Sat Az	-43.1	-81.3	-43.1	-81.3
Measured Shadow	39.8	68.3	13.8	23.3
Height Estimate	**46.9**	**46.5**	**16.3**	**15.9**

The forward looking problem of shadow length prediction from a known building height was then investigated in order to judge its applicability to furthering the automation process of the shadow-based AOD retrieval method. Using the same two scenes and buildings, and assuming the user has access to the 13 September image, the shadow lengths for 27 October are predicted. This simulates the process a user would use to take data from a known image and use the STK forecasted solar and satellite

geometries to predict future shadow lengths before imagery collection. Table 2 shows how the process proceeded, starting with the measured shadow length from 13 September, estimating the building height, then using the 27 October angular information to estimate the shadow length for that day. The final two rows of the table show the absolute and relative differences between the estimated and actual shadow lengths. Again, both shadow lengths can be predicted to within a half meter accuracy. This accuracy is significant in that it is near the threshold of the QB panchromatic resolution of 0.6 meters. The percent error obviously increases with the decrease of building height and corresponding shorter shadows. This suggests that taller buildings and longer shadows are better for analysis, however, in the urban scenes where tall buildings are present it is difficult to encounter a long shadow over a relatively uniform surface that is also unobstructed by adjacent structures.

Table 2. Calculated shadow lengths for the two target buildings on 27 October 2003 are listed along with the measured shadow lengths of 13 September 2003 and geometry used to calculate them from the QuickBird satellite imagery. Difference and error values are compare the calculated values to measured shadow length.

Building 1		**Building 2**	
13 Sep Ls	39.8	13 Sep Ls	13.8
13 Sep Angle	40.3	13 Sep Angle	40.3
Height Est	46.9	Height Est	16.3
27 Oct Angle	55.7	27 Oct Angle	55.7
Ls Estimate	**68.8**	Ls Estimate	**23.9**
27 Oct Ls	**68.3**	27 Oct Ls	**23.3**
Difference	0.5	Difference	0.6
Error (%)	**0.7**	Error (%)	**2.5**

B. AUTOMATING PROGRAM

The unification of the shadow method for AOD retrieval as performed by Vincent (2006) under a single computer program, with user input, was achieved using the IDL programming language in its interface with the ENVI software. The end result is a single program that can be called up in ENVI and run on user-defined ROIs in the current loaded image. The user simply executes the program, is prompted to enter the ROIs

corresponding to the shaded and non-shaded regions, and the program calculates the aerosol optical depth from the information contained in the ROI statistic files. In order to ensure that the process followed was adequately replicating the original shadow method, tests were performed comparing the results of the new program to the results of Vincent (2006). Identical ROIs were used such that the method of computation was the only change in the retrieval process.

1. Multispectral Comparison

The case selected to verify the multispectral automated AOD retrieval method was from Beijing, China on 8 July 2003. This region was specifically chosen for the verification as the automated method's first operational use would be by Evans (2007) on the same location. As is shown in Figure 5, the values on the x-axis represent the AOD output of the streamlined IDL program while the Y-axis values represent the results of Vincent (2006). Each point represents the intersection of the values produced for a single ROI and band. The output of the automated program exactly matched the results of Vincent (2006) for the multispectral ROIs analyzed.

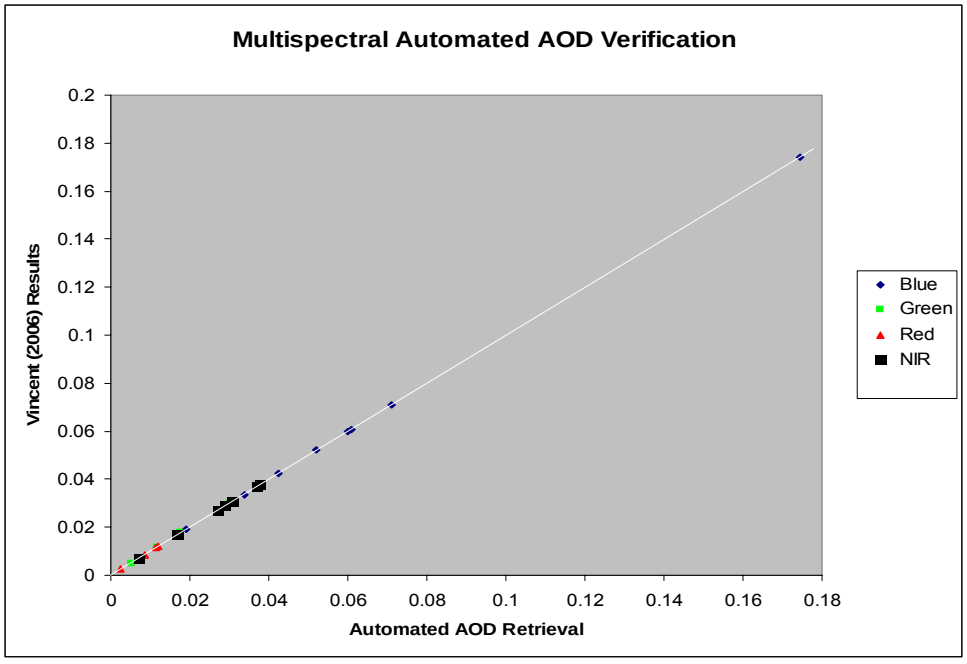

Figure 5. Automated multispectral AOD retrievals are compared to the retrievals of Vincent (2006) for identical shadow and non-shadow regions.

2. Panchromatic Comparison

To validate the automated AOD retrieval program for the QB panchromatic channel, a case was chosen from the United Arab Emirates on 24 September 2004. It was unlikely that the results would exactly match for this case as the calculations performed by Vincent (2006) included a mode value for the shadow region which was hand-selected from a histogram plot of each individual ROI. However, examination of the histogram plots for the shadow regions shows that, for the relatively small pixel sample within each ROI, the mode can represent significant high or low bias and may not adequately describe the true shadow region radiance. In some cases, multiple modes in the histogram plot exist for which the user would then have to manually decide which value was more representative of the shadow radiance. In the automated method, ENVI cannot automatically calculate and properly select the mode of a given ROI. In an effort to further the automation of this process, the automated program was written using the mean of the shaded region to calculate the radiance difference between shadow and non-shadow regions used for AOD retrieval.

What follows is a comparison of the results of the automated retrieval, using the mean values for the shaded region, to the results of Vincent (2006) which use hand-selected mode values for the shaded region radiance. Figure 6 plots the AOD results from the two retrievals using the mean and the mode. The thick red line at 0.4 denotes the actual AOD measured in situ by the Aerosol Robotic Network (AERONET) site. Unexpectedly, the mean values for the two retrieval methods were identical – effectively providing the exact same AOD answer across the sample size. This is purely a numerical manifestation. The two methods do not produce the same AOD for each sample ROI, instead the individual values merely balance out across the sample to produce equal mean values. However, it is intuitive that over a large enough sample the results should be the same because for a shadow with a perfect normal distribution of radiance values, the mean and mode should be equal.

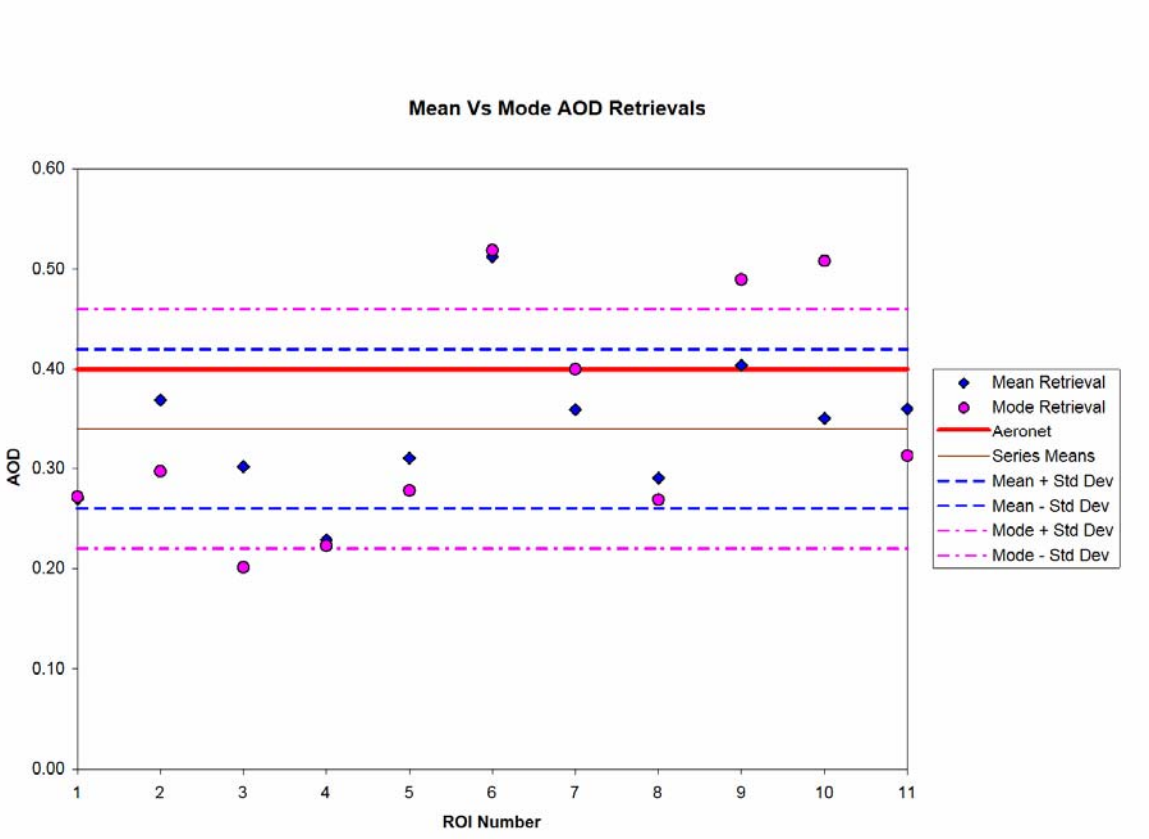

Figure 6. Automated AOD retrievals for the panchromatic band using mean radiance for the shadow regions are compared to the results of Vincent (2006) using the mode radiance for the shadow regions. Individual AOD samples are represented by the blue diamonds (mean) and the pink circles (mode). The actual Aeronet AOD measurement is denoted by the thick red line. The mean retrieved AOD for both methods is represented by the solid brown line. The dashed blue lines represent the standard deviation of the automated retrieval while the dashed pink lines represent the standard deviation of the mode retrieval.

The dashed lines in Figure 6 represent the range of the standard deviation from the mean for the two retrievals. The mean retrieval shows a lower standard deviation seeming to take away some of the variability associated with hand-selecting the mode values. Also evident from the plot is that for each individual ROI, except the one where the mode retrieval hit the AERONET AOD exactly, the mean retrieval AOD value is always closer to the actual AOD value. It is therefore not evident that the modes and means are equivalent for this sample, but instead that the alternating high and low biased

modes balance out across the sample to approximate the sample mean. The values obtained using the mean radiance values provide a more accurate retrieval method by eliminating the bias caused by visually selecting a mode from a small pixel sample size.

C. SHADOW MORPHOLOGY

With an ability to automatically retrieve AOD from shadows in a satellite image, attention is now turned to how best to sample a shadow given its spatial variations. Results from digital photographic images taken on 29 November and 6 December 2006 are best divided into categories based on either the variable of interest or the types of profiles compared. Surface type and shadow-generator color are the variables of interest, and horizontal and vertical profiles are the two delineated types of profiles. A final important category of shadow evolution over time is also examined.

1. Surface Type

The type of surface that a given shadow falls on proves to be a large factor in determining how usable that shadow is for analysis. Figure 7 displays the profiles of three shadow regions from the 6 December images over three different surface types. The profiles extend from the base of the plywood shadow producer out past the end of the shadow. For all three plots, the shadow-generator is oriented horizontally with the white surface facing the shadow region. Brightness count plots for the three bands are indicated by their respective colors on the graphs. The adjacent comparison of these three profiles is necessary to qualitatively compare the way different surface types affect not only the shadow profiles, but also the bands individually. The first and most obvious result is that the non-uniform surface of the old asphalt creates a highly variable profile. This variability leads to a lower difference between the shadow and non-shadow regions rendering it less usable for AOD calculation.

(a)

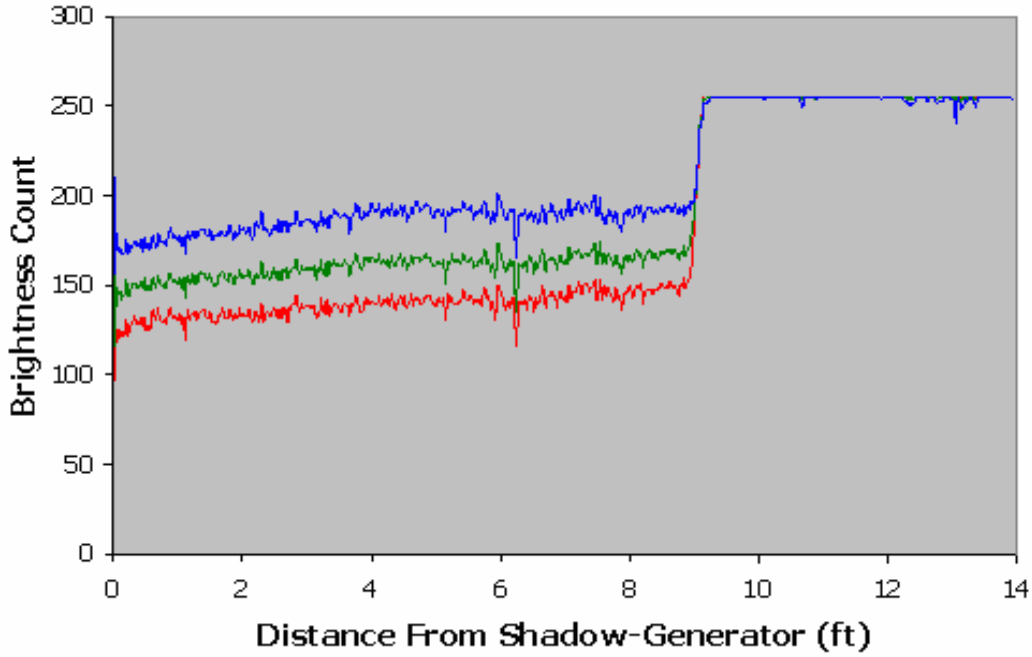
Brightness Count
300
250
200
150
100
50
0
0
2
4
6
8
10
12
14
Distance From Shadow-Generator (ft)

(b)

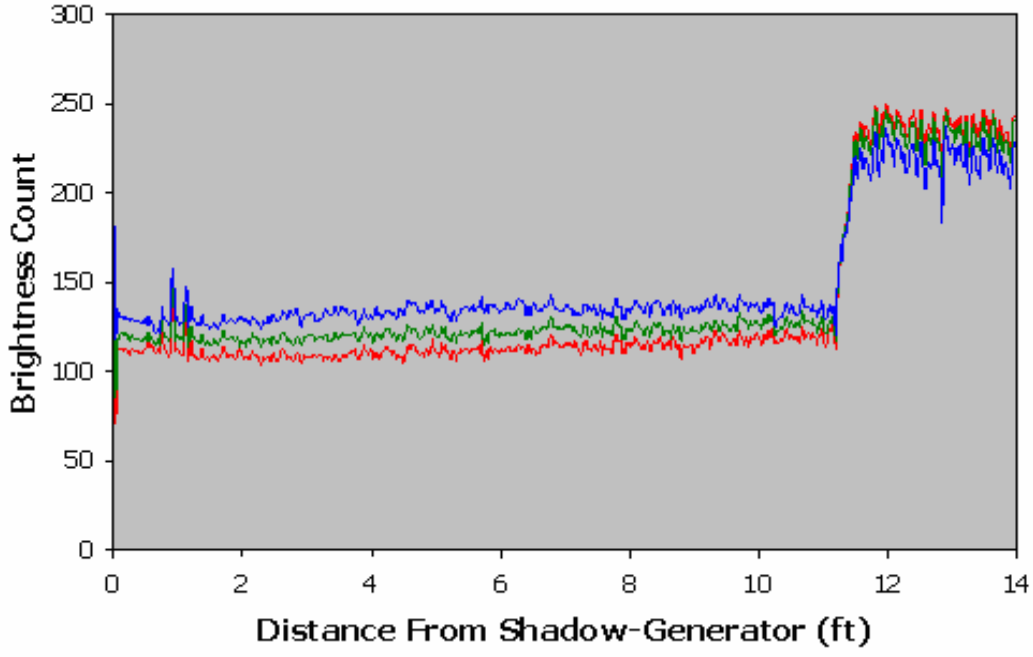
Brightness Count
300
250
200
150
100
50
0
0
2
4
6
8
10
12
14
Distance From Shadow-Generator (ft)

(c)

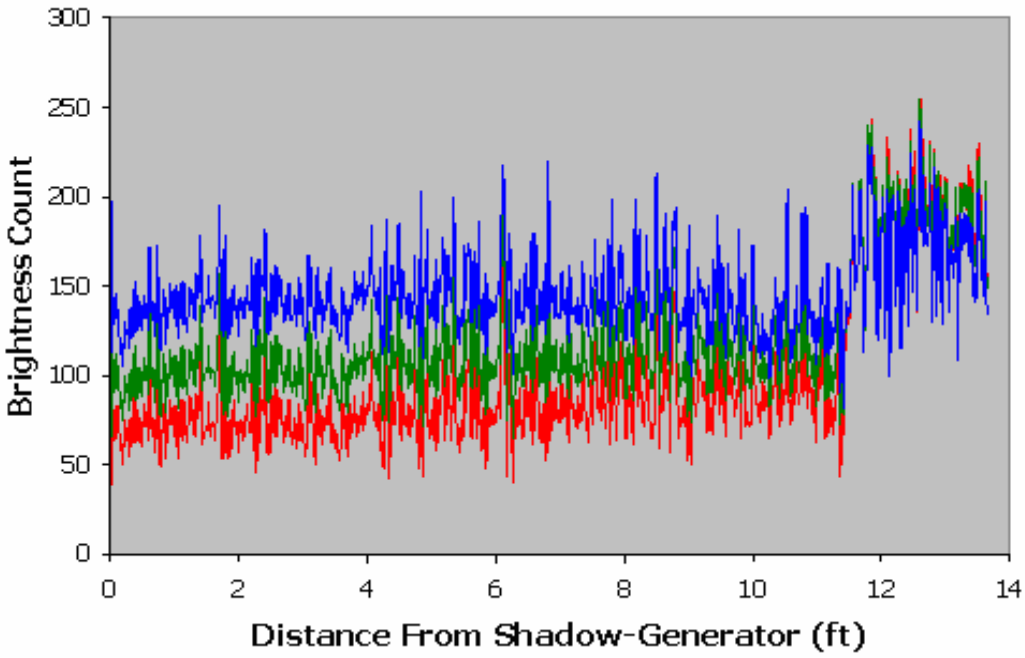

Figure 7. Profiles of brightness count from the center of the shadow-generator base in the horizontal orientation extending into the non-shadow region for the (a) concrete tarmac, (b) asphalt, and (c) old asphalt surface types. The three colored plots represent the red green and blue band-specific brightness counts.

The darker surface provided by the new asphalt provides a tight packing of the three bands within the shadow region. The brighter concrete tarmac surface spreads the bands within the shadow region and displays a saturation characteristic with all bands being equal outside the shadow region. This brighter surface also exhibits a steeper gradient of brightness decrease as the profile approaches the shadow-producing object. A greater brightness difference between the shadow and non-shadow regions is apparent for all bands over the dark asphalt surface, however, quantifying this difference is not possible because of the saturation characteristic evident in the concrete tarmac plot.

2. Shadow-Generator Surface Color

A qualitative comparison identifies a tangible difference between shadow profiles with different shadow-generator surface brightness values. Figure 8 shows brightness

count of all three bands as profiles extending from the base of the shadow-generator for two images over the concrete tarmac. Examining the profiles from shadow-generator base to shadow extent, it is evident that in all cases the profiles trail off in brightness value as the shadow producer is approached. However, a noticeable difference is apparent depending on whether the black or white board surface is directed towards the shadow. The dark surface exhibits a steeper gradient while the white surface gradient is flatter. The difference between the two images in Figure 8 is the surface color of the shadow-generator, and the qualitatively greater brightness decrease due to the black surface versus the white surface is evident.

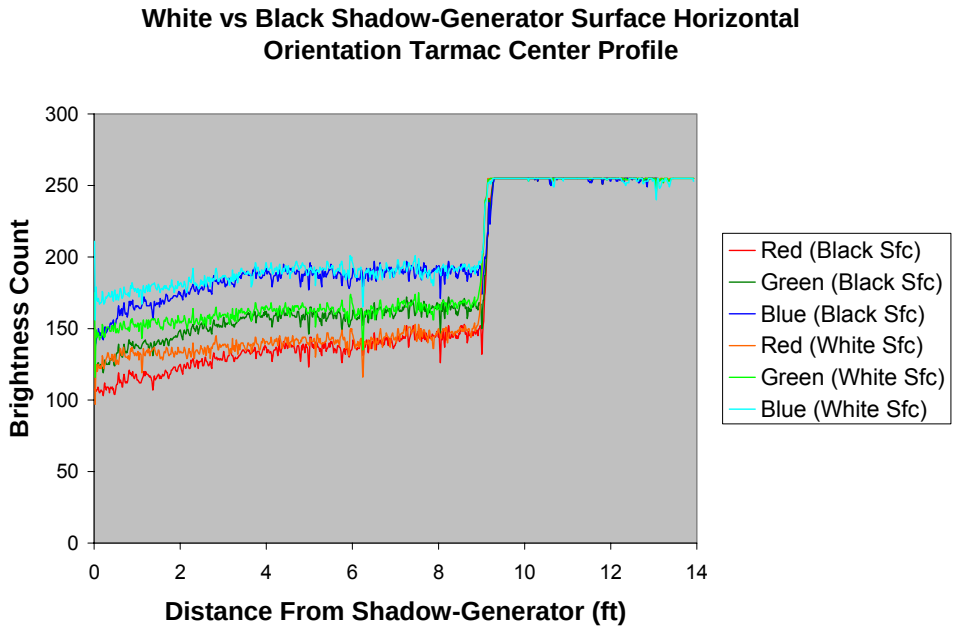

Figure 8. Brightness count profiles extending from center of shadow base to non-shadow region for both dark and light shadow-generator colors.

The physical explanation for the different levels of brightness decrease is that the brighter board surface acts as a reflector. More sky radiance is scattered into the shadow region by the white shadow-generator surface. This additional scattering counteracts the normal radiance decrease due to more of the sky radiance being blocked as the shadow-generator surface is approached. Quantification of this difference caused by the shadow-casting surface's color is difficult because other variables influence the magnitude of its

effect. The difference in slopes between the white and black surface profiles over the brighter concrete is much greater than over the darker asphalt, and for all cases the blue wavelengths are more affected than the others due to the enhancement of Rayleigh scattering by atmospheric gases at shorter wavelengths. The brightness reduction transition occurs at roughly the same distance from the shadow producer regardless of the orientation, and thus the transition zone covers an equal spatial distance of approximately four feet regardless of aspect ratio. Figure 9 shows the almost identical transition zones for both horizontal and vertical orientations of the shadow-generator over the same surface. The vertical orientation shadow region covers a greater spatial extent because of its longer shadow. However, over the region where shadow is present for both orientations, the profiles show a similar brightness trend.

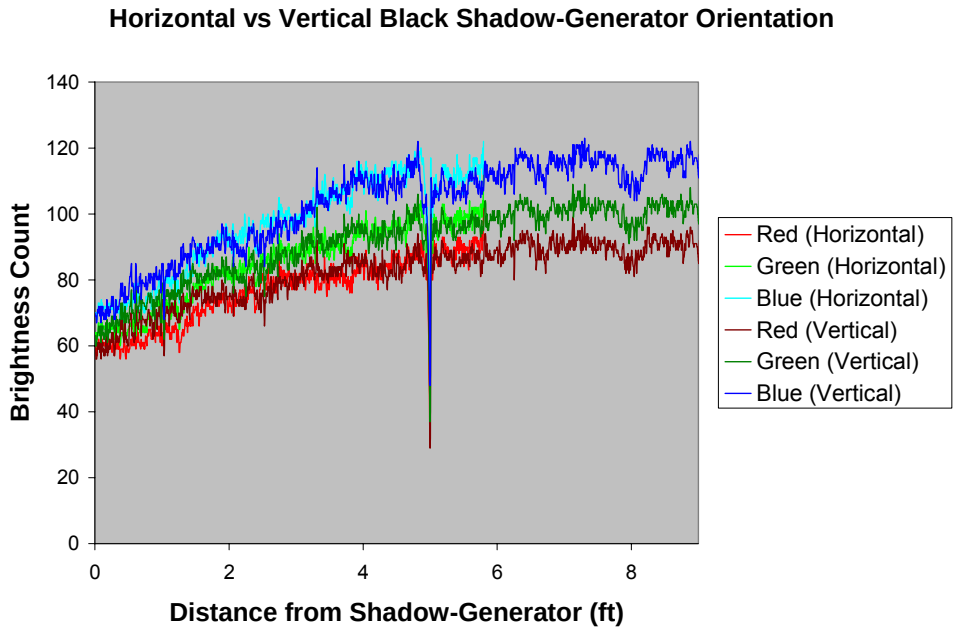

Figure 9. Center profiles of shadow region with dark shadow-generator surface with both horizontal and vertical orientations shown.

The differential brightness decrease between shadows cast by different colored structures can be quantified from this analysis. Though the transition zones covered the same spatial distance regardless of aspect ratio, this distance represented different percentages of the total shadow region. In the horizontal orientation, the transition zone

was evident over approximately half of the shadow region. For the vertical orientation, the nearest 30% of the shadow region was influenced by the transition zone. These individual percentages could be used when examining either horizontally or vertically oriented shadow-generators, however, a better rule of thumb would be to simply avoid collecting radiance values from the half of the shadow nearest to the shadow-casting structure.

3. Horizontal Cross Sections

The three horizontal cross sections taken near the shadow-generator, at the center of the shadow region and at the extent of the shadow region, provide further insight into the previously discussed brightness reduction near the shadow-generator. Also, there is information on the transition zones at the horizontal shadow region edges evident in these profiles. The focus of this analysis is on the horizontal orientation profiles over the new asphalt and concrete tarmac surfaces. The old asphalt surface was too variable and the vertical orientation images had data damaging lens flares in portions of their shadow regions. Qualitatively, the near cross sections for all bands displayed the lowest brightness values. In line with the previous results, the greater brightness difference between shadow edge and shadow onset occurred with the black shadow-generator. To quantify the observed results, the average values across each cross section's shadow region were calculated for each band with the results provided in Table 3. Figure 10 provides a visual representations of the reduction values from Table 3.

Table 3. Average brightness values are shown for center, near, and edge horizontal cross sections of the shadow region. Both colored sides of the shadow-generator are identified over both the concrete tarmac and asphalt surface. Brightness decrease is identified in percent between the cross sections with total decrease representing the brightness loss from the shadow edge to the base of the shadow-generator.

White Horizontal Tarmac	Red	Green	Blue	**Black Horizontal Tarmac**	Red	Green	Blue
Center	141.23	163.34	190.99	Center	135.99	159.65	189.18
Edge	146.43	166.01	191.03	Edge	146.09	165.58	190.55
Near	134.7	154.97	178.88	Near	115.89	139.43	167.3
Edge to Center Decrease (%)	3.55	1.61	0.02	Edge to Center Decrease (%)	6.92	3.58	0.72
Center to Near Decrease (%)	4.63	5.12	6.34	Center to Near Decrease (%)	14.77	12.67	11.56
Total Decrease (%)	**8.01**	**6.65**	**6.36**	Total Decrease (%)	**20.67**	**15.79**	**12.2**
White Horizontal Asphalt	Red	Green	Blue	**Black Horizontal Asphalt**	Red	Green	Blue
Center	111.31	122.8	137.38	Center	108.68	119.24	131.97
Edge	115.33	125.83	139.78	Edge	113.91	124.52	138.39
Near	108.56	118.09	129.62	Near	103.02	109.56	117.31
Edge to Center Decrease (%)	3.48	2.41	1.71	Edge to Center Decrease (%)	4.59	4.24	4.64
Center to Near Decrease (%)	2.47	3.83	5.65	Center to Near Decrease (%)	5.21	8.12	11.11
Total Decrease (%)	**5.87**	**6.15**	**7.26**	Total Decrease (%)	**9.56**	**12.01**	**15.23**

The first obvious difference is that the influence of the shadow-generator surface color is at least double for all bands over either ground surface type as shown by the total percent decrease in brightness from the edge profile to the near profile. Also, the quantitative effect on a specific color band varies as a function of ground surface type. For the concrete tarmac cases shown in the top portion of Table 3, the red wavelengths decrease the most through the profile while they decrease the least over the darker asphalt surface represented in the lower portion of the table. Conversely, blue wavelengths decrease most over the darker asphalt and least over the bright concrete tarmac. These wavelength dependent differences are due to the dominance of red and blue radiance over a brighter, more reflective surface and darker, less reflective surface respectively. The percent reduction in brightness quantified in Table 3 over the different ground surfaces and with the varied shadow-generator color is displayed in Fig. 10. It is clear that the same wavelength dependent trends hold over the different surfaces regardless of the shadow-generator color. Also the greater percent decrease in cases of black shadow-generator surface is easily identified.

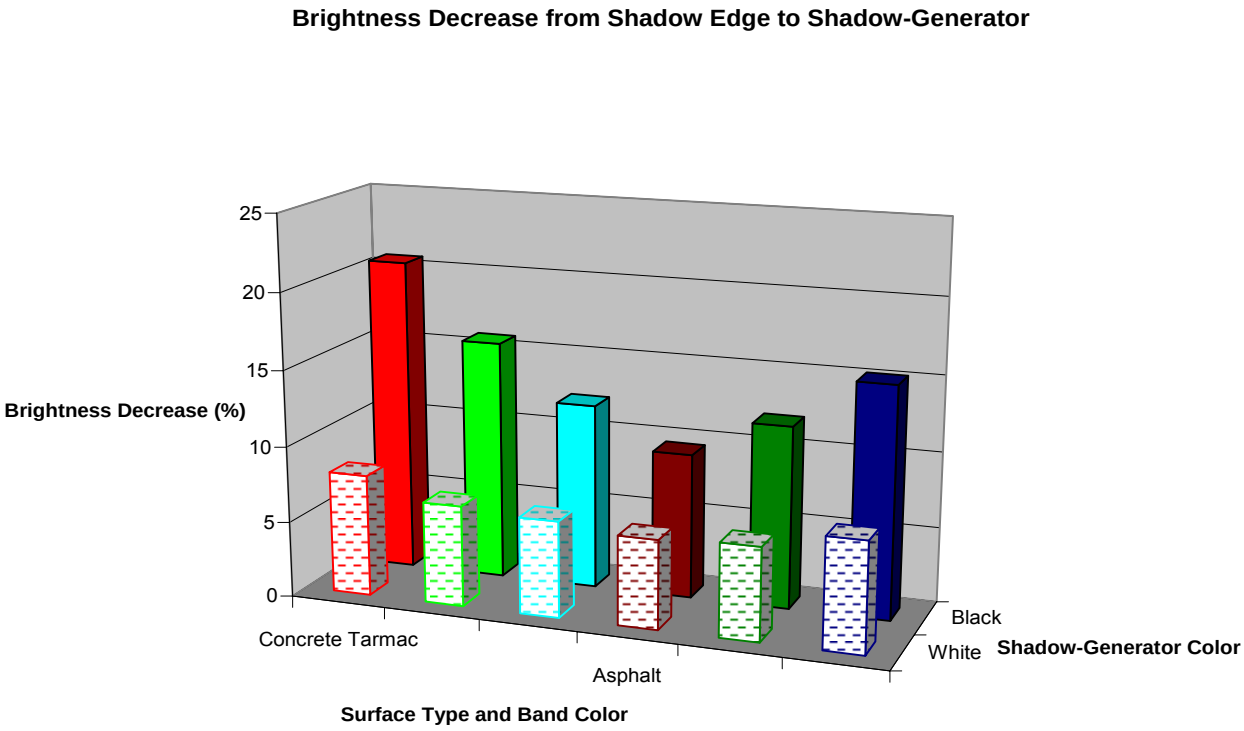

Figure 10. Graphical depiction of brightness decrease in percent from shadow edge to base of shadow-generator. The three bands are noted by the colors in the graph, the two rows represent the different shadow-generator colors, and the left and right three values represent the concrete tarmac surface and the asphalt surface respectively.

4. Vertical Profiles

Vertical profiles of the shadow region were compared in the same manner as the horizontal cross sections using profiles along each edge of the shadow and a center profile. Qualitative inspection of the profiles showed that the center profile always had lower brightness values than the profiles along the edges. Averages of the values for each band within the shadow region along each profile were calculated to compare the brightness lost away from the lateral shadow edges. Table 4 shows the results of this analysis for the horizontal orientations over the concrete tarmac and new asphalt with

both colored sides of the board exposed. Figure 11 provides a visual representation of the values in Table 4, again showing the same band-dependent trends over the different surface types and the greater magnitude of brightness decrease for the black-surfaced shadow generator.

Table 4. Average brightness values are shown for center, left, and right vertical cross sections of the shadow region. Both colored sides of the shadow-generator are identified over both the concrete tarmac and asphalt surface. Brightness decrease is identified in percent between the average of the edge values and the center value.

White Horizontal Tarmac	Red	Green	Blue	**Black Horizontal Tarmac**	Red	Green	Blue
Left	144.63	164.82	190.54	Left	139.99	161.65	188.36
Right	142.13	162.5	188.06	Right	136.06	158.13	185.05
Center	137.96	159.29	185.67	Center	130.08	152.2	180.25
% Less Center	**3.78**	**2.67**	**1.92**	% Less Center	**5.75**	**4.81**	**3.46**
White Horizontal Asphalt	Red	Green	Blue	**Black Horizontal Asphalt**	Red	Green	Blue
Left	115.99	126.97	140.77	Left	112.59	122.96	135.51
Right	116.3	128.55	145.43	Right	113.31	125.62	141.22
Center	112.52	121.63	133.37	Center	108.73	116.9	126.75
% Less Center	**3.12**	**4.80**	**6.80**	% Less Center	**3.74**	**5.94**	**8.40**

The magnitude of the decreases between the lateral edges and the center profiles is in all cases less than the decreases observed between the shadow extent and the shadow producer from the horizontal cross sections. However, the qualitative relationships remain the same. In each case, the red band is most significantly affected over the concrete tarmac and least over the asphalt, with the opposite again being true for the blue band. Surface color of the shadow-generator retains its influence on the decreasing brightness as shown by the right side of Table 4 with greater reduction evident when the black surface is oriented towards the shadow. The magnitude of this influence is decreased, though, because the vertical profiles are averaged over their full extent and the surface color exerts the most influence only over the areas nearer to the shadow-generator.

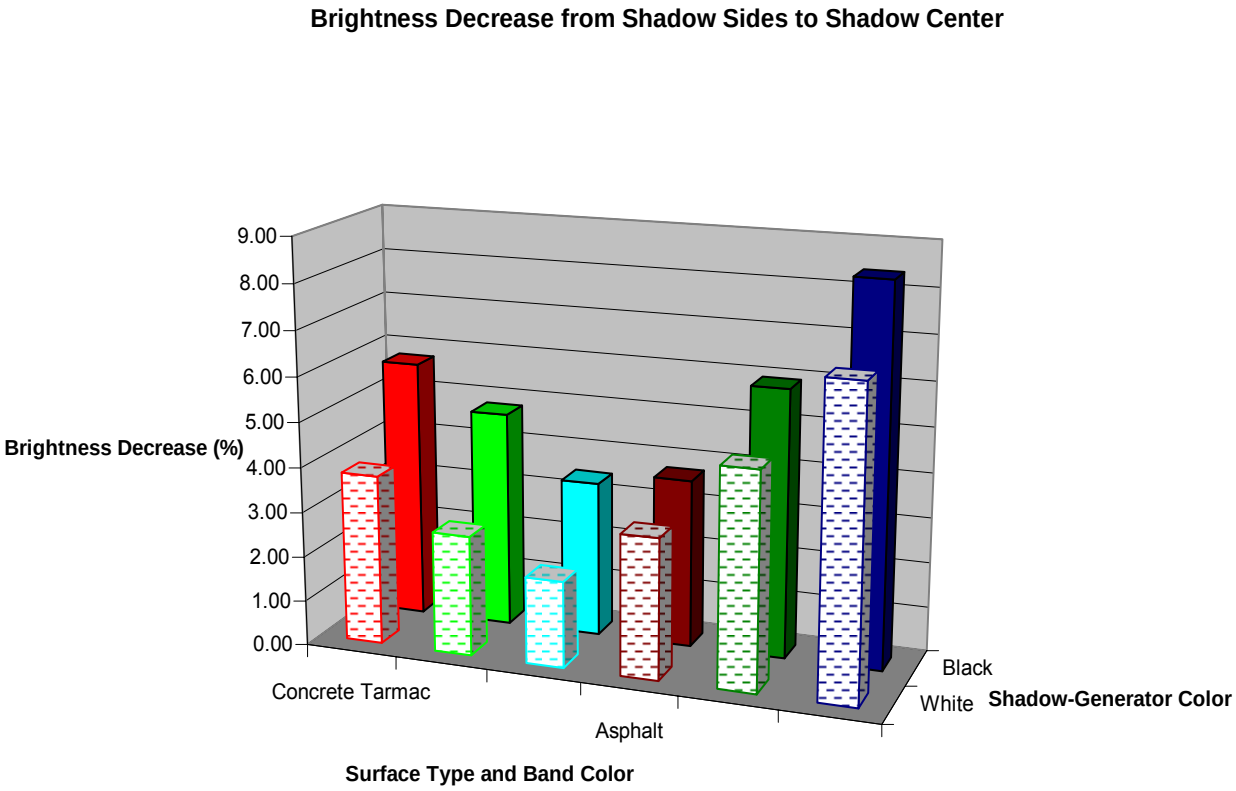

Figure 11. Graphical depiction of brightness decrease in percent from the shadow edges to the center profile. The three bands are noted by the colors in the graph, the two rows represent the different shadow-generator colors, and the left and right three values represent the concrete tarmac surface and the asphalt surface respectively.

5. Shadow Evolution

Investigation of the evolution of the shadow region over time was accomplished by creating three profiles over the same spatial surface trace at three different times an hour apart on the tarmac adjacent to the northeast corner of the CIRPAS hangar. Images taken from the fixed location of the 29 November experiment were used to create the profiles. All images used are from the Canon EOS 20 D with a constant aperture and shutter speed. The first profile from the 1330 image is over the tarmac without shadow, the second is at 1430 after the shadow has encompassed the region, and the third is at

1530 with the region still encompassed by the shadow. Figure 12 shows the plotted comparison of the same profile before and after it is part of the shadow region.

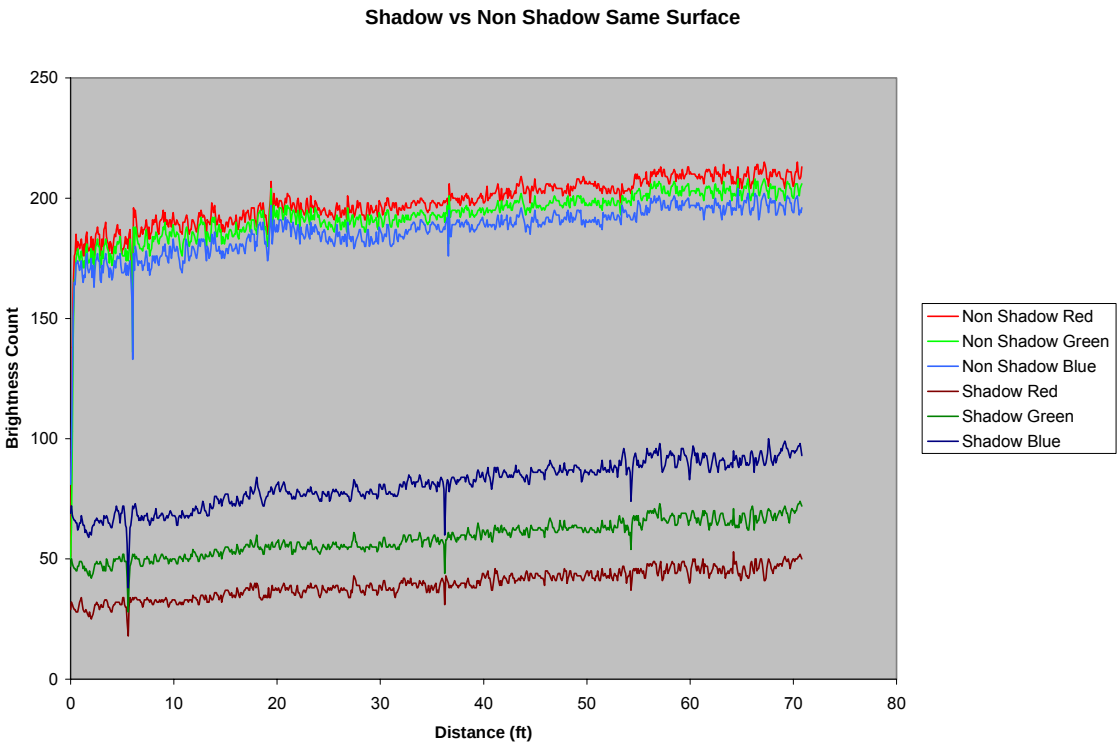

Figure 12. Profiles of the same spatial profile from the concrete tarmac adjacent the CIRPAS hangar before and after the shadow encompasses the region.

From Fig. 12 it is evident by the similar trend of the profiles that a relatively similar brightness increase occurs as the profile extends away from the building. However, the brightness spacing between bands is much greater within the shadow profile. Also, the red band switches from the brightest to darkest values once the shadow overtakes the region while the blue band does the opposite. This shows that the surface preferentially reflects in the longer red wavelengths when the region is exposed to direct solar radiance. The reversal within the shadow region is because only indirect radiance is reaching the surface with blue holding the largest value due to atmospheric Rayleigh scattering.

Figure 13 shows the decrease in brightness within the same region of the shadow at the later time due to the reduction in the solar angle as the day progresses. It is also

evident that this reduction in brightness is nearly uniform throughout the profile as the profile is unchanged in shape at the later time - there is simply a magnitude shift. This shift in magnitude is quantifiable by calculating the mean values of brightness for each band and each profile and then calculating the difference in the means for the corresponding bands at the different imaging times. The results of this calculation show that the brightness reduction affects each band approximately the same with the blue, green, and red bands showing a 15.7, 14.6, and 16.8 % reduction respectively.

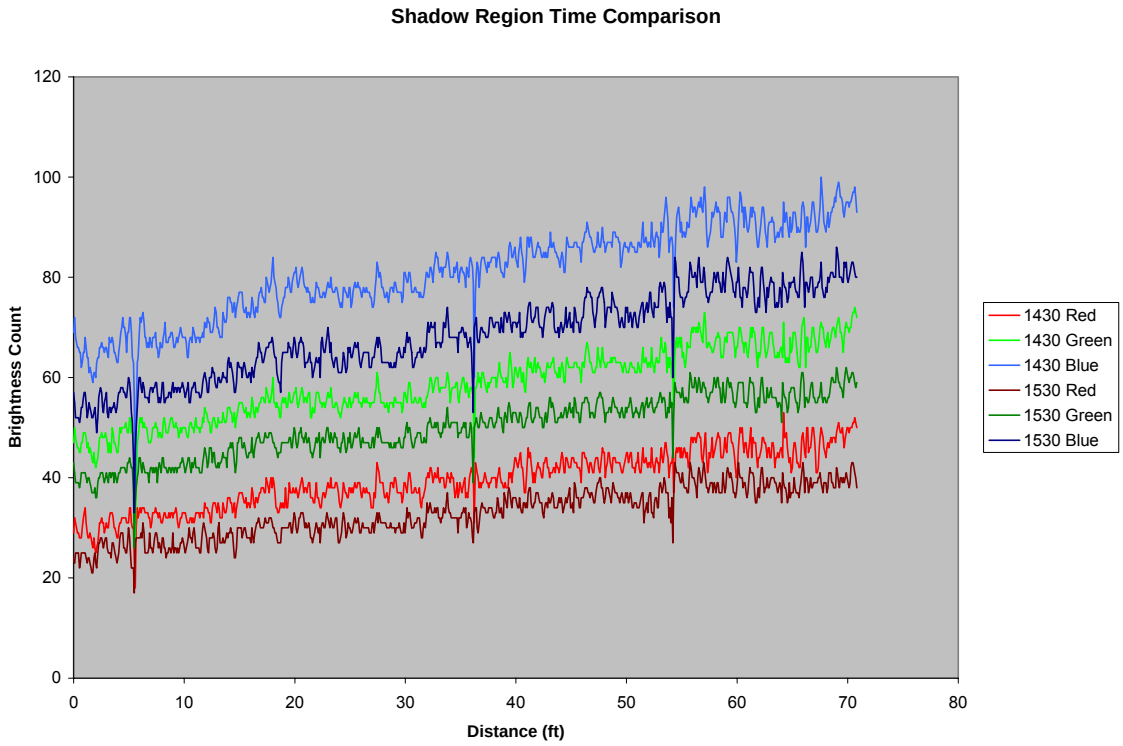

Figure 13. Profiles of the same spatial profile within the shadow region of the concrete tarmac adjacent to the CIRPAS hangar for two different imaging times. The 1430 image is just after the shadow has encompassed the profile, and at the 1530 image time the profile is well inside the shadow region.

THIS PAGE INTENTIONALLY LEFT BLANK

V. CONCLUSIONS AND RECOMMENDATIONS

A. CONCLUSIONS

Investigation of automation techniques for the shadow-based method of aerosol optical depth retrieval provides clear steps that can be taken towards creating an operationally functional iteration of the method. The process of taking the theoretical, research-oriented technique and making it applicable for the day to day operations of the warfighter is lengthy indeed. However, through the improvements in the understanding of shadow regions and the automation of the process calculation method, tangible progress is made in bridging the theoretical to operational gap.

The possibility of shadow length prediction from the satellite imagery is studied using orthorectified QuickBird imagery. Accurate building height prediction from imagery-measured shadow lengths is possible using solar and satellite geometric relationships. These geometric relationships can be combined with the ability to predict future geometric configurations of satellite, sun, and target using the Satellite Tool Kit. This combination of tools allows for the prediction of future shadow lengths from known, or calculated, building heights. The prediction capabilities provide an advantageous tool towards the end state of operational functionality. Not only could a user be able to predict future shadow locations for their area of operations, but also known shadow producers for that area of operations could be programmed into a database for automatic selection of shadow and non-shadow radiance values and calculation of AOD.

The physical automation of the shadow-based AOD calculation process provides perhaps the most visible, tangible, and immediately useful step towards total retrieval automation. The combination of different steps of the calculation method into a single, user-friendly interface within the imagery viewing software provides immediate benefit to continuing research on the method. The calculation processing time and difficulty is decreased which allows for faster and quantitatively more analysis to be done. Also, a tool now exists for the researcher to analyze the retrieved AOD simultaneous with imagery viewing in order to characterize different variables within the imagery that may

alter the retrieved AOD. The comparison of the automated program results to Vincent (2006) showed exact replication for the multispectral retrieval cases. In the panchromatic band, mean radiance values for shadow regions where used instead of mode values, and initial comparison shows improved results. The creation of the automated calculation program now leaves only the selection of shadow and non-shadow regions from the imagery as the only user-modified step in the retrieval.

To close the circuit on the automated process in total, it will be required to program a method for the automatic selection of the shadow and non-shadow regions within the imagery. In order to reach that ultimate goal, the shadow regions themselves must be better understood. Largely qualitative analysis of brightness differences across shadow regions is provided. Brightness count values from digital camera imagery are analyzed to approximate radiance properties across various shadow region profiles. Identifiable differences are clear over different surface types, with different shadow-generator reflectance properties, and as a result of spatial location with respect to the shadow generator. The differential blocking of the celestial dome and the loss of diffuse sky radiance associated with it is the primary explanation for brightness loss within the shadow region. The center profiles extending from the shadow-generator base to the shadow extent characterized this brightness loss as more sky radiance is blocked by the shadow-generator at its middle than at its edges. The brightness loss is also evident between the shadow extent and the shadow-generator base, with more diffuse sky radiance blocked near the base. The color of the shadow-generator is also shown to have an effect as bright surfaces can add a reflection component to the brightness near the base, mitigating the sky blocking influence. With the importance of sky blockage so evident within the shadow region itself, it follows that this influence could also exist due to adjacent structures in a given image. Quantification of this effect will be necessary for analysis to be accurately performed in an operational setting, especially in urban imagery where many structures are present around shadow regions. Optimal radiance sampling should be in adjacent location pairs for which the effective blocking of the celestial dome will be equal for both the shadow and non-shadow regions.

B. RECOMMENDATIONS

Recommendations for future work include two specific investigations to further the overall automation process of the shadow based method. A highly controlled study into shadow morphology is necessary to quantify results viewed qualitatively in this work. At this juncture sufficient automation and tools have been provided for a comprehensive case study of a fixed targeting automation method at a single location.

1. Controlled Shadow Morphology Study

The brightness count values from the digital camera imagery used in the study cannot be expected to quantitatively transfer to radiance values. To actually quantify the differences evident in brightness across shadow regions, a controlled study would be needed where radiance values could be directly derived. A controlled and known value for surface reflectance would be desirable to eliminate all ground surface based influence. Multiple portable shadow-generators would be useful in order to quantify the effect of adjacent structure sky blockage on shadow regions. Ideally, actual satellite imagery collection would be used for the controlled study. However, by mounting an in situ sensor on a crane, the geometry of a satellite pass could be approximated and the angular effects of the view angle from the near-ground imagery collection done in this study could be eliminated. Through quantifying radiance decreases and isolating their sources, correction factors could be then directly applied to future automatic AOD retrieval.

2. Fixed Target Case Study

The automation techniques and guidance presented in this study open the door for an individual case study of a fixed target based shadow-method AOD retrieval test. The fixed target strategy would work for a single location where certain shadow-generators that produce usable shadow regions can be identified. With the shadow-generators identified, multiple satellite imagery scenes could be collected. With multiple images of the fixed shadow-generating targets, their geometry can be analyzed to provide shadow location and length prediction information for future collection times. The automated retrieval program would then be able to sample the shadow and non-shadow regions to

calculate AOD. Furthermore, the local effects of adjacent structures and surface properties could be investigated for the fixed targets to apply specific correction factors and ensure accurate AOD retrieval of the region. Though not the end state solution of a totally transportable comprehensive method, the fixed targeting case study could provide an operational AOD retrieval capability for a single location.

LIST OF REFERENCES

AFRL, 2004. Target Acquisition Weapons Software V3.4. Northrup Grumman.

Analytical Graphics, Inc., cited 2007: Satellite Tool Kit. [Available online at http://www.stk.com]

Ball Aerospace, cited 2006: Ball Global Imaging System 2000. [Available online at http://www.ballaerospace.com/pdf/bgis.pdf]

DigitalGlobe, cited 2006: QuickBird. [Available online at http://www.digitalglobe.com/about/quickbird.html]

Evans, J. R., 2007: A verification of aerosol optical depth retrievals from high resolution satellite imagery. M. S. thesis, Dept. of Meteorology, Naval Postgraduate School, CA, 109 pp.

Falkner, E., 1995: *Aerial Mapping: Methods and Applications.* Lewis Publishers, 322 pp.

Higgins, G. J., P. F. Hilton, R. Shapiro, C. N. Touart, and R. F. Wachtmann, 1989: *Scientific Report 39: Operational Tactical Decision Aids.* Geophysics Laboratory, Air Force Systems Command, Hanscom AFB, MA, 404 pp.

Hsu, N. C., S. C. Tsay, M. D. King, and J. R. Herman, 2004: Aerosol properties over bright-reflecting source regions. *IEEE Trans. Geosci. Remote Sensing*, **42**, 557-569.

Kaufman, Y. J. and R. S. Fraser, 1984: Atmospheric effect on classification of finite fields. *Rem. Sens. Env.*, **15**, 95-118.

Kaufman, Y. J., and J. H. Joseph, 1982: Determination of surface albedos and aerosol extinction characteristics from satellite imagery. *J. Geophys. Res.*, **87**, 1287-1299.

Kaufman, Y. J. and C. Sendra, 1988: Algorithm for automatic atmospheric corrections to visible and near-IR satellite imagery. *Int. J. Remote Sens.*, **9**, 1357-1381.

Kidder, S. Q. and T. H. Vonder Haar, 1999: *Satellite Meteorology: An Introduction.* Academic Press, pp. 466.

Liou, K. N., 2002: *An Introduction to Atmospheric Radiation.* Academic Press, pp. 583.

Martin, J. S., 2004: Aerosol optical depth model assessment with high resolution multiple angle sensors. M. S. thesis, Dept. of Meteorology, Naval Postgraduate School, CA, 53 pp.

Martonchik, J. V., D. J. Diner, R. Kahn, B. Gaitley, and B. N. Holben, 2004: Comparison of MISR and AERONET aerosol optical depths over desert sites. *Geophys. Res. Lett.*, **31**, L1602.

Odell, A. P. and J. A. Weinman, 1975: The effect of atmospheric haze on images of the earth's surface. *J. Geophys. Res.*, **80**, 5035-5040.

Research Systems Inc., 1999: *ENVI Programmer's Guide.* Research Systems Inc., 595 pp.

Tanre, D., M. Herman, and P. Y. Deschamps, 1981: Influence of the background contribution upon space measurements of ground reflectance. *Appl. Opt.*, **20**, 3676-3684.

Tanre, D., P. Y. Deschamps, C. Devaux, and M. Herman, 1988: Estimation of Saharan aerosol optical thickness from blurring effects in Thematic Mapper data. *J. Geophys. Res.*, **93**, 15955-15964.

Veefkind, J. P., G. de Leeuw, P. Stammes, and R. B. A. Koelemeijer, 1998: Regional distribution of aerosol over land derived from ATSR-2 and GOME. *Rem. Sens. Env.*, **74**, 377-386.

Vincent, D. A., 2006: Aerosol optical depth retrievals from high-resolution commercial satellite imagery over areas of high surface reflectance. PhD Dissertation, Dept. of Meteorology, Naval Postgraduate School, CA, 197 pp.

INITIAL DISTRIBUTION LIST

1. Defense Technical Information Center
   Ft. Belvoir, Virginia

2. Dudley Knox Library
   Naval Postgraduate School
   Monterey, California

3. Chairman, Code MR
   Department of Meteorology
   Naval Postgraduate School
   Monterey, California

4. Professor Philip A. Durkee (Code MR/De)
   Department of Meteorology
   Naval Postgraduate School
   Monterey, California

5. Kurt E. Nielsen
   Department of Meteorology
   Naval Postgraduate School
   Monterey, California

6. 2LT Ryan M. Dombrock
   Department of Meteorology
   Naval Postgraduate School
   Monterey, California